JACS
JOURNAL OF THE AMERICAN CHEMICAL SOCIETY

Communication

pubs.acs.org/JACS

# Protein Induces Layer-by-Layer Exfoliation of Transition Metal Dichalcogenides

Guijian Guan,[†,‡] Shuangyuan Zhang,[‡] Shuhua Liu,[‡] Yongqing Cai,[†] Michelle Low,[‡] Choon Peng Teng,[‡] In Yee Phang,[‡] Yuan Cheng,[†] Koh Leng Duei,[‡] Bharathi Madurai Srinivasan,[†] Yuangang Zheng,[‡] Yong-Wei Zhang,*[,†] and Ming-Yong Han*[,‡]

[†]Institute of High Performance Computing, A*STAR, 1 Fusionopolis Way, 138632 Singapore

[‡]Institute of Materials Research and Engineering, A*STAR, 3 Research Link, 117602 Singapore

Supporting Information

**ABSTRACT:** Here, we report a general and facile method for effective layer-by-layer exfoliation of transition metal dichalcogenides (TMDs) and graphite in water by using protein, bovine serum albumin (BSA) to produce single-layer nanosheets, which cannot be achieved using other commonly used bio- and synthetic polymers. Besides serving as an effective exfoliating agent, BSA can also function as a strong stabilizing agent against reaggregation of single-layer nanosheets for greatly improving their biocompatibility in biomedical applications. With significantly increased surface area, single-layer $MoS_2$ nanosheets also exhibit a much higher binding capacity to pesticides and a much larger specific capacitance. The protein exfoliation process is carefully investigated with various control experiments and density functional theory simulations. It is interesting to find that the nonpolar groups of protein can firmly bind to TMD layers or graphene to expose polar groups in water, facilitating the effective exfoliation of single-layer nanosheets in aqueous solution. The present work will enable to optimize the fabrication of various 2D materials at high yield and large scale, and bring more opportunities to investigate the unique properties of 2D materials and exploit their novel applications.

Since the pioneering discovery and extensive investigation of graphene,[1] single- and few-layer nanosheets of transition metal dichalcogenides (TMDs) have also been attracting great attention due to their semiconducting characteristic, sizable bandgap, large surface area, and promising applications in sensing, catalysis, and composite and energy storage.[2−4] Through breaking weak van der Waals forces between adjacent layers in TMDs, the exfoliated nanosheets confine their electrons to adopt wave function in 2D and turn the indirect bandgap of bulk into the direct one (1.2 to 1.9 eV for single-layer $MoS_2$).[5] Over the past years, a great deal of effort has been made to develop various approaches for reliable and scale-up production of atomically thin TMD nanosheets.[6−12] Among them, micromechanical cleavage has been widely applied to produce single- and few-layer TMD flakes of high purity and cleanliness in limited quantity.[6,7] Liquid-phase routes have also been demonstrated by directly sonicating TMDs in properly selected solvents such as *N*-methylpyrrolidone,[8] dimethylformamide,[9] and a mixture of ethanol and water,[10] which can exfoliate TMDs and also stabilize the resultant nanosheets due to their close surface energies. The method has recently been extended to produce few-layered TMDs by the use of surfactants (e.g., sodium cholate) in water[11] or polymers (e.g., polystyrene) in tetrahydrofuran.[12] Currently, Li-ion intercalation is used to produce single-layer TMDs with organic alkaline metal compounds such as organolithiumand[13−15] and sodium naphthalenide[16] in organic solvents, which usually result in structural and electronic deformations of TMD nanosheets from their bulk.[17] So far, it is very challenging to readily produce highly dispersed single-layer TMD nanosheets in solutions, which will be of importance to study the physical and chemical properties of TMDs and exploit their novel applications. In this research, we demonstrated a cumulative layer-by-layer exfoliation route to produce single-layer $MoS_2$ nanosheets in aqueous solution at high yield by using specific protein, bovine serum albumin (BSA) as an effective exfoliating agent. The resultant single-layer nanosheets are stabilized against reaggregation via the strong binding of BSA, exhibiting good biocompatibility, high binding capacity to pesticides, and large specific capacitance. This protein exfoliation process has been further extended to produce other single-layer TMD nanosheets and graphene.

Experimentally, 50 mg of $MoS_2$ powder was first dispersed in 10 mL of distilled water containing 10 mg of BSA. After sonicating in a sonic bath for 48 h, single-layer $MoS_2$ nanosheets were obtained in water after removing nonexfoliated $MoS_2$ (Figure S1a). The BSA-dispersive $MoS_2$ nanosheets are very stable after storing for a year, and their high dispersibility was not influenced when changing pH from 0 to 14 (Figure S2). The $MoS_2$ nanosheets were first imaged by low-resolution transmission electron microscope (TEM) to show the presence of extremely thin 2D flakes with an average size of 100 × 120 nm (inset of Figure 1a). Their high-resolution TEM image clearly shows hexagonally symmetric structure of $MoS_2$ (Figure 1a). The lattice spacing of 0.27 nm is assigned to (100) atomic planes of $MoS_2$.[9] Fast Fourier transform shows the hexagonal spot pattern (inset in Figure 1a). These indicate that the obtained $MoS_2$ nanosheets were not damaged during sonication,[10] retaining their single crystalline nature.[15] The high-resolution TEM image

**Received:** March 17, 2015
**Published:** May 2, 2015





DOI: 10.1021/jacs.5b02780
J. Am. Chem. Soc. 2015, 137, 6152−6155

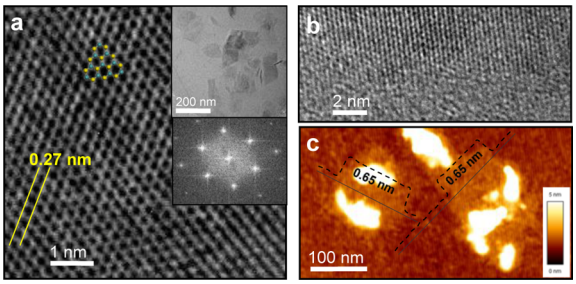


**Figure 1.** High-resolution TEM images of single-layer $MoS_2$ nanosheet at (a) its center and (b) edge exfoliated by using BSA. Insets are the corresponding low-resolution TEM image and fast Fourier transform pattern. (c) AFM image of single-layer $MoS_2$ with a thickness of 0.65 nm.

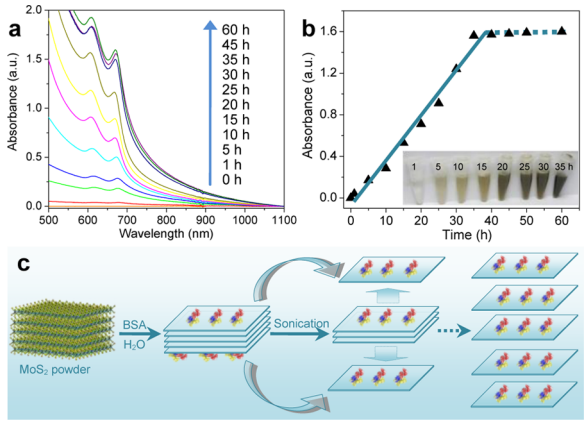


**Figure 2.** (a) UV−vis absorption spectra of the exfoliated $MoS_2$ nanosheets in water after sonication for different times. (b) Temporal evolution of the absorption intensity at 666 nm with the increase of sonication time. Inset is the optical images of the exfoliation solutions after different sonication time. (c) Schematic for the BSA-induced exfoliation of single-layer $MoS_2$ nanosheets under sonication.

at the edge of nanosheets was observed to exhibit the formation of single-layer nanosheets (Figure 1b). Atomic force microscopy (AFM) imaging further confirmed the production of single-layer $MoS_2$ nanosheets with the thickness of 0.65 nm (Figure 1c).[18] The adsorbed BSA was easily distinguished from the underlying $MoS_2$ layer as light spot, which was measured to be ∼10 nm in average (Figure S3). The exfoliation from bulk $MoS_2$ to single-layer $MoS_2$ nanosheets was further demonstrated by their X-ray diffraction (XRD) (Figure S4a). The XRD pattern of the single-layer $MoS_2$ nanosheets did not show any of the reflection peaks from bulk $MoS_2$, indicating that there is no stacking of layers along *c* direction (i.e., the production of single-layer nanosheets).[15] Furthermore, a fluorescent emission at 678 nm appeared after the exfoliation of bulk $MoS_2$ to single-layer nanosheets, due to the transition from indirect to direct band (Figure S4b).[7]

Furthermore, Raman spectrum of single-layer $MoS_2$ nanosheets was measured to give bands at 382 and 408 $cm^{-1}$ (Figure S5), which are associated with the in-plane vibration ($E^1_{2g}$) and out-of-plane vibration ($A_{1g}$) modes, respectively.[19] In addition, UV−vis absorption spectrum of single-layer $MoS_2$ nanosheets clearly exhibits two peaks at 605 and 666 nm (Figure S1b), which are attributed to the direct excitonic transitions at the K point of Brillouin zone.[20] In comparison to bulk $MoS_2$, the absorption peak of single-layer $MoS_2$ blue-shifts from 687 to 666 nm (Figure S6) due to the great decrease in the number of layers.[21] The absorption peak of BSA at 278 nm is clearly observed after dilution for five times (Figure S1b), indicating the formation of BSA-adsorbed $MoS_2$ nanosheets. The mass measurement showed that 6.19 mg of BSA was bound to 13.61 mg of $MoS_2$ nanosheets (the weight ratio of BSA and $MoS_2$ is 45%, in agreement with the estimated one by thermogravimetric analysis in Figure S7). The resulting concentration of $MoS_2$ nanosheets in water was calculated to be 1.36 mg/mL with an exfoliation yield at 27.2%, which is much higher than 0.3 mg/mL obtained by using *N*-methylpyrrolidone,[9] and 0.5 mg/mL by using surfactants.[11] It is estimated that there are ∼120 BSA on each nanosheet, exhibiting that each BSA of 56 $nm^2$ takes up ∼100 $nm^2$ on the surface. In addition, the bound BSA can be partially removed via more rounds of high speed centrifugation with water via centrifugal force, and this process will cause some reaggregation of the $MoS_2$ nanosheets due to the lack of the surface-protective BSA. Here one can see that BSA is an effective exfoliating and stabilizing agent for producing highly dispersible single-layer nanosheets in water through its binding on $MoS_2$.

When sonicating $MoS_2$ powder to produce nanosheets, UV−vis absorption spectra of the resulting $MoS_2$ nanosheets were monitored at the predetermined time interval (Figure 2a). The absorption intensity of $MoS_2$ nanosheets was quickly increased in the first 35 h and then leveled off, reaching the equilibrium in exfoliating $MoS_2$ nanosheets. Figure 2b clearly showed the linear relationship of the absorption intensity with sonication time. One can see that the amount of exfoliated $MoS_2$ nanosheets linearly increased with sonication time within the first 35 h (Figure S1c shows the linear relationship between the absorption intensity and the amount of exfoliated $MoS_2$ nanosheets), indicating the layer-by-layer exfoliation of bulk $MoS_2$ into single-layer nanosheets. The exfoliation rate is calculated to be ∼7.5 × $10^{12}$ single-layer $MoS_2$ nanosheets per hour. Through the experimental observation and temporal evolution, the following process is proposed to exfoliate $MoS_2$ powder for the formation of single-layer $MoS_2$ nanosheets in water (Figure 2c). After adding $MoS_2$ into BSA solution, BSA molecules are stably bound to the surface of $MoS_2$ crystals via the strong hydrophobic interaction, while polar groups of BSA are exposed externally in water (refer to theoretical simulation below). Upon sonication, the surface layer of $MoS_2$ crystals adsorbed with BSA can slide gradually and irreversibly as the freshly exposed surfaces are immediately covered by free BSA, eventually leading to the exfoliation of bulk $MoS_2$ into the single-layer $MoS_2$ nanosheets in water (Figure S8).[22] The exfoliating process proceeds repeatedly with sonication time to produce high-yield single-layer $MoS_2$ nanosheets in water. The single-layer $MoS_2$ nanosheets are conveniently obtained in aqueous solution of BSA at a concentration of less than 2 mg/mL, while the multilayered nanosheets are produced at concentrations of ∼2−4 mg/mL. There are no dispersed nanosheets to be produced at higher concentration of BSA due to the severe self-aggregation of BSA (Figure S9−S14). It is noted that the layer-by-layer exfoliation is only achieved under sonication with low energy density by using a sonic bath instead of a sonic tip (Figure S15).

Besides BSA, other polymers including poly(acrylic acid) (PAA) and polyvinylpyrrolidone (PVP) were also used to exfoliate $MoS_2$ powder under the identical procedure for applications (Figures S16 and S17). First, different polymer-adsorbed $MoS_2$ nanosheets were tested with colorimetric MTT assay (Figure 3a).[23] Single-layer BSA-bound $MoS_2$ nanosheets ($MoS_2$−BSA) showed much higher viability of fibroblast cells


DOI: 10.1021/jacs.5b02780
J. Am. Chem. Soc. 2015, 137, 6152−6155

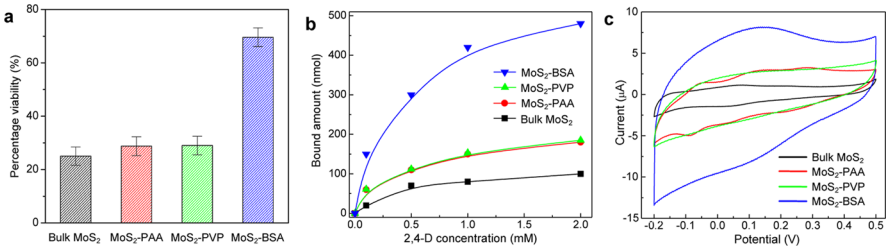


**Figure 3.** Biocompatibility, adsorption, and capacitance of single-layer $MoS_2$–BSA nanosheets in comparison with bulk $MoS_2$ and other polymer-adsorbed $MoS_2$ nanosheets. (a) Biocompatibility of bulk $MoS_2$ and various polymer-adsorbed $MoS_2$ nanosheets via MTT assay. (b) Bound amount of 2,4-DA at different concentrations on bulk $MoS_2$ and various polymer-adsorbed $MoS_2$ nanosheets. (c) Cyclic voltammetry curves of bulk $MoS_2$ and various polymer-adsorbed $MoS_2$ nanosheets at scan rate of 100 mV/s.

than PAA-adsorbed, PVP-adsorbed $MoS_2$ nanosheets ($MoS_2$–PAA, $MoS_2$–PVP), and bulk $MoS_2$, indicating its high biocompatibility for potential biomedical applications. With extremely high surface-to-volume area, the single-layer $MoS_2$ nanosheets possess high-capacity absorption of toxic and hazardous targets (Figure S18). Figure 3b shows that the bound amounts increased in an order of $MoS_2$–BSA > $MoS_2$–PAA ≈ $MoS_2$–PVP > bulk $MoS_2$ at different concentration of 2,4-DA. Interestingly, the bound amounts by $MoS_2$–BSA increased much faster with the increase of 2,4-DA concentration than other materials, exhibiting its much higher binding capacity for target accumulation and solution assay.[24] Furthermore, the cyclic voltammetry curves were measured by using $MoS_2$-coated glass carbon electrode as working electrode (Figure 3c), exhibiting that the $MoS_2$–BSA nanosheets have the largest specific capacitance.[25,26] The specific capacitance of $MoS_2$–BSA nanosheets is 36 F/g at scan rate of 100 mV/s (Figure S19), which is 2.8, 3.0, and 9.0 times as high as that of $MoS_2$–PAA, $MoS_2$–PVP, and bulk $MoS_2$, respectively. Moreover, the specific capacitance of $MoS_2$–BSA nanosheets is greatly larger than that of pure BSA (Figure S20), indicating the major contribution came from single-layer $MoS_2$ nanosheets. In addition, the specific capacitance increased with the decrease of the scan rate (Figure S21). At 5 mV/s, the capacitance of $MoS_2$ nanosheets reached 180 F/g, which is larger than the reported value of 106 F/g for the $MoS_2$ flakes-constructed microspheres.[26]

To understand the exfoliation of $MoS_2$ nanosheets, density functional theory (DFT) was used to simulate the binding energies of special groups of BSA on $MoS_2$ layer (Figure 4a and

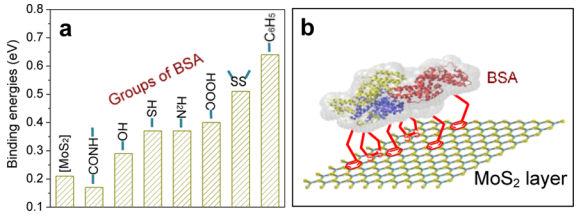


**Figure 4.** Binding of BSA on $MoS_2$ layer. (a) Comparison on the binding energies of different functional groups of BSA on $MoS_2$ layer. [$MoS_2$] is the binding energy between two adjacent $MoS_2$ layers. (b) Schematic for the binding of BSA on $MoS_2$ layer with benzene rings and disulfides.

Table S2). Each BSA contains 583 amino acids (Table S1),[27] including 27 phenylalanine and 35 cysteine that can form 17 disulfide bonds while retaining one free thiol group. The binding energies of the nonpolar benzene rings and disulfides on $MoS_2$ layer are 0.64 and 0.51 eV (Figure 4a), which are much larger than those of polar groups including carboxyl, amino, thiol, hydroxyl, and amide groups. Therefore, the benzene rings and disulfides can more strongly bind on the $MoS_2$ nanosheets via hydrophobic interaction (Figure 4b), while the polar groups of BSA are externally exposed to water. It was demonstrated that after adding BSA and $MoS_2$ powder in water, the nonpolar benzene rings and disulfides of BSA can thus stably bind on the layered $MoS_2$, facilitating the exfoliation to form the BSA-adsorbed $MoS_2$ nanosheets under sonication (Figure S8). This is definitely benefited from the much smaller binding energy between two neighboring $MoS_2$ layers (0.21 eV) than the binding energies of BSA on $MoS_2$ layers.

The simulation and analysis above can further be used to understand the exfoliation of $MoS_2$ nanosheets by using other additive agents. With polar groups, small molecules, including glutathione, methacrylic acid, glycine, and citric acid, did not show their ability to exfoliate $MoS_2$ nanosheets in water due to their weak binding affinity to $MoS_2$ (Figure 4a). Similar results were obtained when using benzoic acid, phenylacetic acid, aniline, phenethylamine, and phenylalanine that possess both polar groups and nonpolar benzene rings. These molecules can bind on $MoS_2$ with the benzene rings (Figure S22), but $MoS_2$ cannot be exfoliated under sonication due to their small molecular weight. It can see that the large molecular weight of BSA plays an important role in the exfoliation of single-layer nanosheets. In comparison to BSA, the synthetic and biopolymers including PAA, PVP, chitosan, and gelatin produced a lower concentration of $MoS_2$ nanosheets (Figure S16). Also, these polymers produced multilayered $MoS_2$ nanosheets (Figure S17) due to the absence of strongly hydrophobic segments. Similarly, other proteins like fibroin without benzene rings[28] did not successfully produce single-layer $MoS_2$ nanosheets as well.

The protein exfoliation can be extended to other layered materials. As revealed by DFT simulation, the benzene rings and disulfides also have higher binding affinity to $WS_2$ layers (Figure S23). So, BSA has ability to effectively exfoliate $WS_2$ crystals. TEM observations show the morphology of nanosheets and the lattice fringe of 0.27 nm corresponds to (100) planes of $WS_2$ (Figure S24a,b).[29] UV–vis absorption spectrum of $WS_2$ nanosheets exhibits a strong peak at 629 nm from $WS_2$ (Figure S24c).[30] The absence of XRD peaks of bulk $WS_2$ indicates the production of single-layer $WS_2$ nanosheets (Figure S24d). Similarly, the benzene rings also have much higher binding affinity to $WSe_2$ layers as compared to other groups (Table S3), facilitating the effective exfoliation of $WSe_2$ nanosheets. Overall, protein exfoliation is a general approach to exfoliate various TMD nanosheets in water.

Furthermore, graphite was successfully exfoliated into graphene with the use of BSA in water and further explained by DFT simulation (Figures S25 and S26). The benzene rings


DOI: 10.1021/jacs.5b02780
J. Am. Chem. Soc. 2015, 137, 6152–6155

have much higher binding affinity to TMD nanosheets as compared to other groups including peptide bonds (Figure 4a). Interestingly, the nonpolar peptide bonds possess much higher binding affinity to graphene as compared to other groups including benzene rings (Figure S25). This shows that the peptide bonds play a major role in the exfoliation of graphene, whereas the benzene rings and disulfides are more important to form single-layer TMDs. As BSA comprises all the benzene rings, disulfides, and peptide bonds, it can exfoliate both TMDs and graphite to their nanosheets. In comparison, fibroin only effectively exfoliated graphite to graphene, while it cannot successfully exfoliate TMDs. This is because fibroin comprises a large number of peptide bonds in its backbones but does not contain benzene rings.[28]

In conclusion, we report a facile and general method for effectively exfoliating various layered materials (e.g., $MoS_2$, $WS_2$, $WSe_2$, and graphite) in water by using BSA into single-layer nanosheets. It was demonstrated that BSA was adsorbed on $MoS_2$ layers to greatly improve biocompatibility. Moreover, the BSA-bound $MoS_2$ layers exhibit a higher binding capacity to pesticides and a larger specific capacitance. The protein-induced layer-by-layer exfoliation process was revealed by various control experiments and DFT simulations. It is interesting to find that benzene rings and disulfide groups of protein have much higher binding affinity to TMD nanosheets, while peptide bonds have much higher binding affinity to graphene as compared to other groups. As a consequence, BSA can effectively exfoliate various TMDs and graphite into monolayer nanosheets. In contrast, other proteins like fibroin can only exfoliate graphite into graphene. The present work will enable the optimization of the fabrication of more 2D materials, provide insights to better understand their physical and chemical properties, and offer more opportunities for their applications.

## ■ ASSOCIATED CONTENT

### Supporting Information

Synthetic methods, sample characterizations, exfoliation mechanism, BSA and $MoS_2$ concentration effect, and production of $WS_2$ nanosheets and graphene. The Supporting Information is available free of charge on the ACS Publications website at DOI: 10.1021/jacs.5b02780.

## ■ AUTHOR INFORMATION


### Corresponding Authors

*zhangyw@ihpc.a-star.edu.sg
*my-han@imre.a-star.edu.sg


### Notes

The authors declare no competing financial interest.

## ■ REFERENCES


(1) (a) Novoselov, K. S.; Geim, A. K.; Morozov, S. V.; Jiang, D.; Zhang, Y.; Dubonos, S. V.; Grigorieva, I. V.; Firsov, A. A. *Science* **2004**, *306*, 666. (b) Novoselov, K. S.; Fal'ko, V. I.; Colombo, L.; Gellert, P. R.; Schwab, M. G.; Kim, K. *Nature* **2012**, *490*, 192. (c) Geim, A. K. *Science* **2009**, *324*, 1530. (d) Mei, Q.; Zhang, Z. *Angew. Chem., Int. Ed.* **2012**, *51*, 5602.

(2) (a) Chhowalla, M.; Shin, H. S.; Eda, G.; Li, L. J.; Loh, K. P.; Zhang, H. *Nat. Chem.* **2013**, *5*, 263. (b) Ding, Q.; Meng, F.; English, C. R.; Cabán-Acevedo, M.; Shearer, M. J.; Liang, D.; Daniel, A. S.; Hamers, R. J.; Jin, S. *J. Am. Chem. Soc.* **2014**, *136*, 8504.

(3) (a) Lopez-Sanchez, O.; Lembke, D.; Kayci, M.; Radenovic, A.; Kis, A. *Nat. Nanotechnol.* **2013**, *8*, 497. (b) Lukowski, M. A.; Daniel, A. S.; Meng, F.; Forticaux, A.; Li, L.; Jin, S. *J. Am. Chem. Soc.* **2013**, *135*, 10274. (c) Yoo, D.; Kim, M.; Jeong, S.; Han, J.; Cheon, J. *J. Am. Chem. Soc.* **2014**, *136*, 14670.

(4) Nicolosi, V.; Chhowalla, M.; Kanatzidis, M. G.; Strano, M. S.; Coleman, J. N. *Science* **2013**, *340*, 1226419.

(5) (a) Mak, K. F.; Lee, C.; Hone, J.; Shan, J.; Heinz, T. F. *Phys. Rev. Lett.* **2010**, *105*, 136805. (b) Cao, T.; Wang, G.; Han, W.; Ye, H.; Zhu, C.; Shi, J.; Niu, Q.; Tan, P.; Wang, E.; Liu, B.; Feng, J. *Nat. Commun.* **2012**, *3*, 887.

(6) (a) Novoselov, K. S.; Jiang, D.; Schedin, F.; Booth, T. J.; Khotkevich, V. V.; Morozov, S. V.; Geim, A. K. *Proc. Natl. Acad. Sci. U.S.A.* **2005**, *102*, 10451. (b) Tongay, S.; Zhou, J.; Ataca, C.; Liu, J.; Kang, J. S.; Matthews, T. S.; You, L.; Li, J.; Grossman, J. C.; Wu, J. *Nano Lett.* **2013**, *13*, 2831. (c) Li, H.; Yin, Z.; He, Q.; Li, H.; Zhang, Q.; Zhang, H. *Small* **2012**, *8*, 682. (d) Mouri, S.; Miyauchi, Y.; Matsuda, K. *Nano Lett.* **2013**, *13*, 5944.

(7) Splendiani, A.; Sun, L.; Zhang, Y.; Li, T.; Kim, J.; Chim, C.-Y.; Galli, G.; Wang, F. *Nano Lett.* **2010**, *10*, 1271.

(8) O'Neill, A.; Khan, U.; Coleman, J. N. *Chem. Mater.* **2012**, *24*, 2414.

(9) (a) Coleman, J. N.; Lotya, M.; O'Neill, A.; et al. *Science* **2011**, *331*, 568. (b) Ou, J. Z.; Chrimes, A. F.; Wang, Y.; Tang, S.-Y.; Strano, M. S.; Kalantar-zadeh, K. *Nano Lett.* **2014**, *14*, 857.

(10) Zhou, K.-G.; Mao, N.-N.; Wang, H.-X.; Peng, Y.; Zhang, H.-L. *Angew. Chem., Int. Ed.* **2011**, *50*, 10839.

(11) Smith, R. J.; King, P. J.; Lotya, M.; Wirtz, C.; Khan, U.; De, S.; O'Neill, A.; Duesberg, G. S.; Grunlan, J. C.; Moriarty, G.; Chen, J.; Wang, J.; Minett, A. I.; Nicolosi, V.; Coleman, J. N. *Adv. Mater.* **2011**, *23*, 3944.

(12) May, P.; Khan, U.; Hughes, J.; Coleman, J. N. *J. Phys. Chem. C* **2012**, *116*, 11393.

(13) (a) Joensen, P.; Frindt, R. F.; Morrison, S. R. *Mater. Res. Bull.* **1986**, *21*, 457. (b) Zhu, C.; Zeng, Z.; Li, H.; Li, F.; Fan, C.; Zhang, H. *J. Am. Chem. Soc.* **2013**, *135*, 5998.

(14) (a) Chou, S. S.; De, M.; Kim, J.; Byun, S.; Dykstra, C.; Yu, J.; Huang, J.; Dravid, V. P. *J. Am. Chem. Soc.* **2013**, *135*, 4584. (b) Wang, L.; Xu, Z.; Wang, W.; Bai, X. *J. Am. Chem. Soc.* **2014**, *136*, 6693.

(15) (a) Matte, H. S. S. R.; Gomathi, A.; Manna, A. K.; Late, D. J.; Datta, R.; Pati, S. K.; Rao, C. N. R. *Angew. Chem., Int. Ed.* **2010**, *49*, 4059. (b) Eda, G.; Yamaguchi, H.; Voiry, D.; Fujita, T.; Chen, M.; Chhowalla, M. *Nano Lett.* **2011**, *11*, 5111.

(16) Zheng, J.; Zhang, H.; Dong, S.; Liu, Y.; Nai, C. T.; Shin, H. S.; Jeong, H. Y.; Liu, B.; Loh, K. P. *Nat. Commun.* **2014**, *5*, 2995.

(17) Gordon, R. A.; Yang, D.; Grozier, E. D.; Jiang, D. T.; Frindt, R. F. *Phys. Rev. B* **2002**, *65*, 125407.

(18) Radisavljevic, B.; Radenovic, A.; Brivio, J.; Giacometti, V.; Kis, A. *Nat. Nanotechnol.* **2011**, *6*, 147.

(19) Zeng, Z.; Yin, Z.; Huang, X.; Li, H.; He, Q.; Lu, G.; Boey, F.; Zhang, H. *Angew. Chem., Int. Ed.* **2011**, *50*, 11093.

(20) Quinn, M. D. J.; Ho, N. H.; Notley, S. M. *ACS Appl. Mater. Interfaces* **2013**, *5*, 12751.

(21) Sreedhara, M. B.; Matte, H. S. S. R.; Govindaraj, A.; Rao, C. N. R. *Chem.—Asian J.* **2013**, *8*, 2430.

(22) Yang, P.; Liu, F. *J. Appl. Phys.* **2014**, *116*, 014304.

(23) Lu, Y. C.; Chen, J.; Wang, A. J.; Bao, N.; Feng, J. J.; Wang, W.; Shao, L. *J. Mater. Chem. C* **2015**, *3*, 73.

(24) Guan, G.; Wang, S.; Zhou, H.; Zhang, K.; Liu, R.; Mei, Q.; Wang, S.; Zhang, Z. *Anal. Chim. Acta* **2011**, *702*, 239.

(25) Feng, J.; Sun, X.; Wu, C.; Peng, L.; Lin, C.; Hu, S.; Yang, J.; Xie, Y. *J. Am. Chem. Soc.* **2011**, *133*, 17832.

(26) Krishnamoorthy, K.; Veerasubramani, G. K.; Radhakrishnan, S.; Kim, S. J. *Mater. Res. Bull.* **2014**, *50*, 499.

(27) Guan, G.; Liu, S.; Cai, Y.; Low, M.; Bharathi, M. S.; Zhang, S.; Bai, S.; Zhang, Y. W.; Han, M. Y. *Adv. Mater.* **2014**, *26*, 3427.

(28) Zhou, C. Z.; Confalonieri, F.; Jacquet, M.; Perasso, R.; Li, Z. G.; Janin, J. *Proteins* **2001**, *44*, 119.

(29) Rao, C. N. R.; Matte, H. S. S. R.; Maitra, U. *Angew. Chem., Int. Ed.* **2013**, *52*, 13162.

(30) Zhao, W.; Ghorannevis, Z.; Chu, L.; Toh, M.; Kloc, C.; Tan, P. H.; Eda, G. *ACS Nano* **2013**, *7*, 791.




DOI: 10.1021/jacs.5b02780
*J. Am. Chem. Soc.* 2015, 137, 6152−6155